

A Novel Shallow Bore Ground Heat Exchanger for Ground Source Heat Pump Applications—Model Development and Validation

Joseph Warner¹, Xiaobing Liu^{2*}, Liang Shi³, Ming Qu³, Mingkan Zhang²

¹University of Tennessee, USA

²Oak Ridge National Laboratory, USA

³Purdue University, USA

* Corresponding author

Abstract

A novel ground heat exchanger design, the Underground Thermal Battery (UTB), was proposed as a low-cost alternative to the conventional vertical bore ground heat exchanger (VBGHE) for the application of ground source heat pumps (GSHPs). The UTB is designed to be installed in a shallow borehole (less than 6 m deep) and thus could cost much less than the conventional VBGHE, which usually is installed in vertical bores 60 m deep. By utilizing natural convection of water and phase change materials, the UTB tempers its temperature change in response to thermal loads, which helps improve the efficiency of GSHPs. A one-dimensional (1D) model of the UTB has been developed and validated with the measured performance data of a small-scale UTB, as well as the simulation results of a more detailed three dimensional (3D) numerical model, which accounts for both heat transfer and fluid dynamics in the UTB. This 1D model is computationally much more efficient than the 3D model and thus can simulate the annual performance of the UTB with acceptable computation time. The 1D model has been used to evaluate the performance of the UTB so that it can be compared with the conventional VBGHE.

KEYWORDS

Ground Source Heat Pump; Ground Heat Exchanger; Numerical Modeling; Validation

NOMENCLATURE

Symbol	Description	Units
T	temperature	C
c_p	heat capacity	J/kg · K
ρ	density	kg/m ³
q_{soil}	Heat transfer to soil	J
q_{HEX}	Heat transfer from heat exchanger	J
q_{PCM}	Heat transfer to PCM	J

V_{tank}	volume of UTB tank	m^3
\vec{r}_s	Soil node vector	-
P	Logarithmic power of soil node distribution	-
\vec{u}	Base vector for soil nodes	-
n_s	Number of soil nodes	-
r	Radial coordinate	m
Δr	Special increment	m
Δr_{min}	Minimum special increment for stability	m
α	Thermal diffusivity	m^2/s
Δt	Simulation time step	s
Δt_c	Stability time step	s
C	Effective heat capacity	J/kgK
c_l	Liquid PCM heat capacity	J/kgK
c_s	Solid PCM heat capacity	J/kgK
θ	Ratio of solid to liquid PCM	-

1. INTRODUCTION

It was estimated that residential and commercial buildings contributed 40% of all United States energy consumption in 2010, 43% of which can be attributed to heating, ventilation, and air conditioning (HVAC) (D&R International 2012). This implies that approximately 17% of the total energy consumption in the United States is a result of residential and commercial HVAC. Furthermore, fossil fuels such as natural gas are often used for space heating. Energy efficient alternatives to conventional HVAC technology are desired to reduce this energy consumption, and the associated greenhouse gas emissions. The ground source heat pump (GSHP) is an energy efficient technology for space heating, cooling and air conditioning. Approximately 6 billion BTUs of primary energy can be saved annually in the United States by retrofitting existing heating and cooling systems with GSHPs (Liu et al. 2019). The high efficiency of GSHPs is a result of the favorable subsurface temperature of the ground, which is cooler than ambient air in summer but warmer than ambient air in winter. However, the adoption of GSHPs in the United States is currently limited by their high cost of installation. The ground heat exchanger (GHE), which is used to exchange heat with the surrounding ground formation, accounts for about 30% of the total installation cost of a GSHP system (NYSERDA 2017). The most commonly used GHE in the United States is the vertical bore ground heat exchanger (VBGHE), and the expensive drilling required to create the borehole is the primary factor contributing to the high cost of VBGHE installation (Liu et al. 2018).

There have been efforts to reduce the cost of the GHE, primarily with the aim of increasing its heat transfer performance so that the total length of the borehole can be reduced. An example of this is various heat exchanger loop designs, such as a double U-tube loop, coaxial pipe, and multiple loops twisted together (Jensen 2014). Other improvements include thermally enhanced grouting materials (Tiedje and Guo 2013), high-performance working fluids (Palm and Ignatowicz 2016), and improved heat exchanger pipe materials (Gonthier et al. 2012). However, the small dimensions of the borehole relative to the surrounding ground formation limit the potential for performance improvements, as the ground is the dominant factor in the heat transfer. Also, while some of these approaches moderately improve the performance, they also increase the cost. An assessment of the cost reduction potential of GHE concluded that improving borehole heat transfer itself usually resulted in less than 20% cost reduction (Liu et al. 2018) and it was thus recommended that new, innovative GHE designs, which can provide similar performance while requiring less drilling, should be investigated. The horizontal ground heat exchanger is another common method for exchanging heat with the ground. A horizontal ground heat exchanger consists of straight pipes or spiral pipes (e.g., in a slink shape) buried just a few feet below the surface, and it can provide similar performance as the VBGHE (CDH 2017, Im et al. 2012) but with a lower cost. However, horizontal ground heat exchangers require a large land area and significant excavation to install. Other shallow ground heat exchangers have also been explored. One example is the basket heat exchanger. A basket heat exchanger consists of a helical coil wrapped around supporting rods and buried in the soil. The helical heat exchanger has a large surface area per unit depth. Field tests of three basket heat exchangers found that it was a viable method for meeting heating and cooling loads (Bertermann et al. 2018). However, the basket heat exchangers are highly sensitive to the thermal conductivity of the backfill material and the surrounding soil. Several basket heat exchangers are required to match the heating and cooling capacity of a single borehole due to their relatively low heat transfer capacity (i.e., interfacing with a relatively small volume of soil). Another approach of shallow GHE is the GeoColumn. It utilizes a shallow tank of water to transfer heat to the ground. A heat exchanger coil transfers heat from a refrigerant to the tank and the inner column promotes natural convection within the tank. The water in the tank gives this design a larger heat capacity than the conventional VBGHE. However, the cost and performance of this design has not been thoroughly investigated, especially for longer terms. In addition, this design requires a large amount of refrigerant to fill the heat exchanger and may have difficulty for the lubricating oil returning to the compressor.

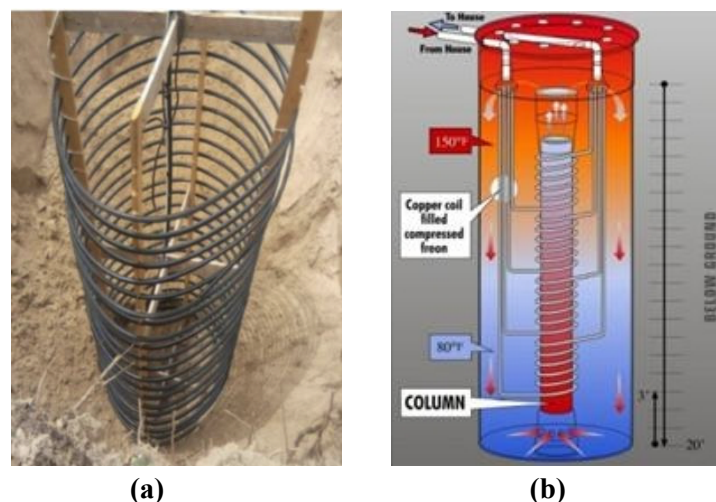


Figure 1. (a) basket heat exchanger (Bertermann et al. 2018); and (b) GeoColumn (Cordts 2011)

A new design of GHE, named as underground thermal battery (UTB), is proposed to achieve the performance of a conventional VBGHE but at a significantly lower cost. A one-dimensional numerical model of the UTB is developed to predict its performance so that it can be compared with the conventional VBGHE. The model development and validation are presented in this paper, along with a preliminary performance and cost analysis of the UTB.

2. UNDERGROUND THERMAL BATTERY

The underground thermal battery (UTB) was invented at Oak Ridge National Laboratory as an alternative to the conventional VBGHE. As depicted in Figure 2, a UTB is comprised of a tank filled with water, which is buried in the shallow subsurface of the ground (less than 6 m deep). A helical heat exchanger is immersed in the center of the tank and connected to a water source heat pump. A phase change material (PCM) is suspended in the annulus between the heat exchanger and the tank wall to provide additional thermal capacity to the tank. A unique “water chimney” design utilizes the vertical temperature gradient of the heat exchanger coil (warm at bottom and cold at top) to promote natural circulation within the tank, increasing the heat transfer between the tank water and the surrounding soil, heat exchanger coil, and the PCM, while maintaining a relatively uniform tank temperature. The tank has a large heat capacity due to the sensible heat of the water and the latent heat of PCM. This large heat capacity reduces the temperature response rate of the tank water for a given heat input, and thus maintains the outlet temperature of the UTB within a narrower range than the conventional VBGHE. The heat absorbed by (or extracted from) the water and the PCM can dissipate into (or be recovered from) the ground through the tank wall. The tank water can be replaced (e.g., by integrating with a lawn irrigation system or a rainwater harvest system), or conditioned with other natural heat sinks (e.g., ambient air) or heat sources (e.g., solar thermal), through an optional second heat exchanger.

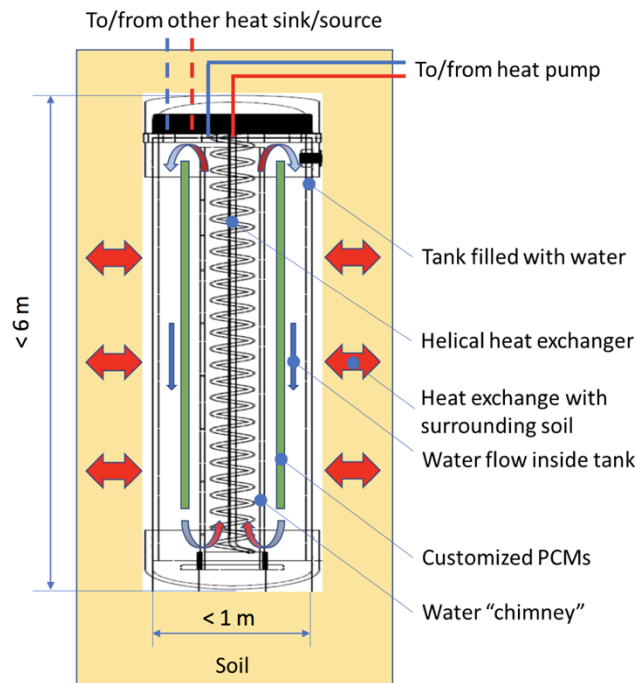


Figure 2. Schematic of an Underground Thermal Battery

The shallow bores (< 6 m depth) required for installing UTBs can be drilled with an auger drill rig, which is less expensive than the rotary drill rig or the downhole hammer used for drilling the relatively deep (>60 m depth) vertical bores for the conventional VBGHEs (Zacchei 2016). Because the installation of a UTB requires much less drilling and the drilling can be done with a less expensive auger drill rig, a significant cost reduction can be expected if the UTB can have the same performance as the conventional VBGHE.

2.1 Small-scale UTB prototype

A small-scale prototype, as shown in Figure 3, was developed to characterize the performance of the UTB under controlled laboratory conditions. Table 1 lists the dimensions a conventional VBGHE, a full size UTB, and the small-scale UTB. The diameter and depth of the small-scale prototype is scaled down with a 1:5 ratio from that of the full scale UTB. The 1:5 ratio was determined by the allowed height of the experimental apparatus at the lab. The height of the small-scale UTB prototype is 1.2 m (4 ft), which is 1/5 of the proposed height of the full-size UTB (6.1 m or 20 ft). Similarity theory was used to determine the heat input and flow rate of the heat carrier fluid in the small-scale UTB prototype, which ensures the temperature response of the small-scale UTB is similar to the full-size UTB.

Table 1. Full and Lab-scale dimensions for UTB prototype.

Dimension	VBGHE borehole	Full-scale UTB	Small-scale UTB
Depth (m.)	61	6.1	1.2
Diameter (m.)	0.15	1	0.2
Volume (m ³)	1.11	5.45	0.04
Surface Area (m ²)	29.2	20.4	0.92

The water tank of the small-scale UTB is made with acrylic and the thickness of the tank wall is 8.2 mm. A helical heat exchanger made with 6.4 mm diameter copper tube is placed at the center of the tank and is enclosed with a 10.7 cm diameter plastic tube. The tube promotes natural convection in the tank by creating a “chimney effect”. It also allows thermocouples to be suspended throughout the tank for distributed temperature measurements. Three PCM panels curved into a hollow-cylinder shape are suspended in the annulus between the inner tube and the tank wall. The height of the PCM cylinder is 2/3 of the tank height, and the thickness of each PCM panel is 3.81 mm. The PCM is made with a mixture of salt hydrates and its melting temperature is 23°C. While the relevant thermophysical properties of the PCM are known (Table 3), the chemical composition of salt hydrates is proprietary information of the PCM vender. While a GSHP system usually operates in heating or cooling mode at different times of a year, the size of a GHE is usually determined by the more dominant load between heating and cooling. The PCM is used to add heat capacity of the GHE at the more dominant loading condition so that the size of the GHE can be reduced. It is possible to use two PCMs that have different melting temperatures—a lower temperature for heating mode and a higher temperature for cooling mode. The total amount of the PCMs and the mixing ratio of the PCMs with different melting temperatures need to be optimized to reduce the overall cost of the UTB.

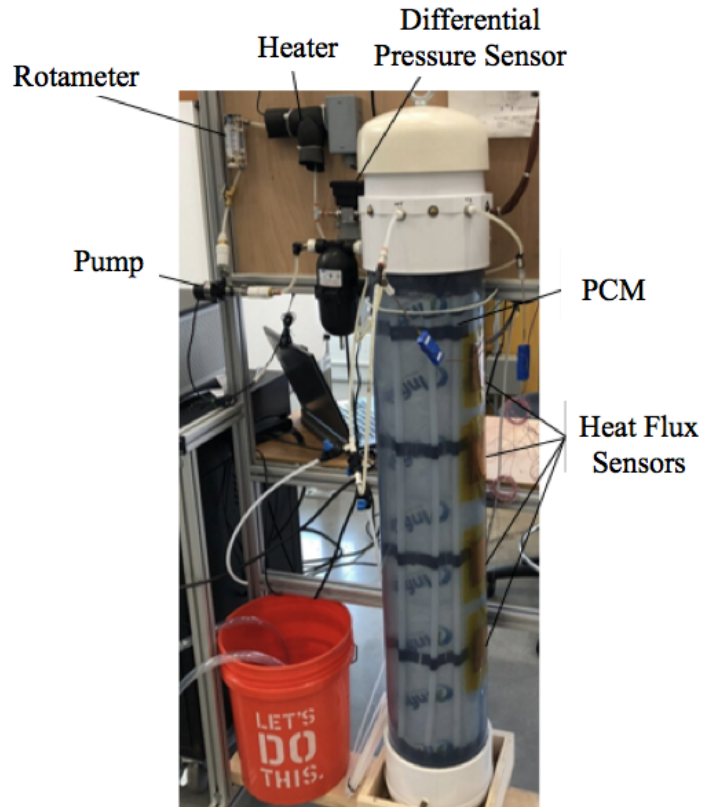


Figure 3. A small-scale prototype of the underground thermal battery

2.2 Experimental apparatus

An experimental apparatus was constructed to test a small-scale UTB prototype. Figure 4 shows the schematic of the experimental apparatus, which include a circulating pump, an electric heater, a sand tank, and a data acquisition system. The pump circulates water in the helical heat exchanger at a constant flow rate. The heater provides constant heat input to the UTB at a predefined schedule. A sand tank (Figure 4) was constructed to emulate the shallow subsurface of the ground. The sand tank (1.2 m. diameter and 1.55 m. height) is filled with dry sand, which has a thermal conductivity of 0.46 W/m-K. The outside of the sand tank is insulated. The data acquisition system records following measurements at 1-minute interval during a test.

- Flow rate, inlet and outlet temperature, and differential pressure of the helical heat exchanger
- Heat flux at the tank wall, which is measured with four evenly distributed heat flux sensors on the outer surface of the tank wall as shown in Figure 3.
- Temperatures at various locations inside the UTB and the sand tank. The temperature sensors are suspended vertically in six groups. The first group is inside the inner tube of the UTB, the second is in the middle of the UTB annulus, the third is on the inside wall of the UTB. The fourth is on the outside wall of the UTB, the fifth is in the center of the sand tank annulus, and the sixth is on the inside wall of the sand tank. They are numbered in a coordinate system which increases radially from the center of the UTB to the edge of the sand tank, and vertically from the bottom of the tank to the top, as shown in Figure 4.

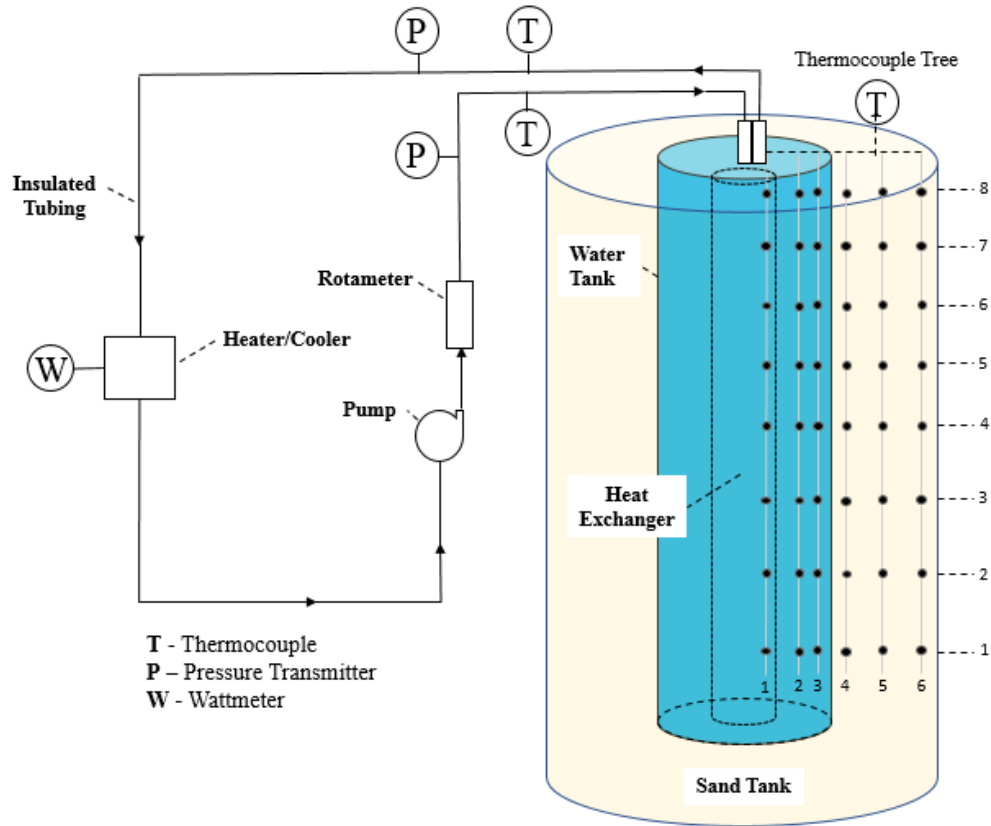


Figure 4. Schematic of the experimental apparatus for testing a small-scale UTB

3. MODEL DEVELOPMENT

Various analytical and numerical models for the VBGHE have been developed over the years, including an analytical model based on the infinite length line source theory (Ingersoll et al. 1954), a hybrid numerical and analytical model developed by Eskilson and Claesson (1988), a thermal resistance and capacity model (TRCM) introduced by Al-Khoury et al. (2005). A few models were also developed to model the short-term (e.g., sub-hour) temperature response of a VBGHE, such as a two-dimensional finite volume numerical model developed by Yavuzturk (1999) and an analytical solution developed by Lamarche and Beauchamp (2007), which accounted for the heat transfer within the heat exchanger pipe.

The above existing models cannot simulate the performance of a UTB because they do not model the transient heat transfer inside the tank, especially the natural convection of water in the tank and the phase change process of the PCM. As a part of this project, a three-dimensional (3D) transient heat transfer and fluid dynamic model of the UTB has been developed and validated by Zhang et al. (2019). However, because of the large size of the simulation domain and the detailed numerical calculations of the 3D model, it is too time consuming to perform long-term (e.g., annual) simulations of the UTB. A simplified version of this model is thus needed to predict the long-term performance of a UTB in response to seasonal thermal loads of a GSHP system. The development of a simplified one-dimensional (1D) transient heat transfer model of the UTB is introduced in this section.

3.1 Assumptions and Simplifications

The simulation domain of the UTB and its surrounding soil is cylindrical symmetric along the vertical axis of the UTB. Therefore, the heat transfer problem is simplified from three-dimensional to two-dimensional (radial, vertical along the depth). In addition, it is assumed that the tank water temperature and the soil temperature are uniform along the depth of the UTB. Therefore, the heat transfer problem is further simplified as one-dimensional in the radial direction.

The 1D model was developed based on following assumptions, which are commonly used for modeling ground heat exchangers:

1. Homogenous and constant thermal properties of the soil
2. Perfect contact between the UTB wall and the surrounding soil (i.e., no contact resistance)

The model simplified the water tank as a cylinder with uniform temperature. This simplification is consistent with the measured temperature profile inside the small-scale UTB. Figure 5 shows the measured temperature profile of the small-scale UTB during a test when 75 W heat was continuously rejected to the tank for five hours. Figure 5(a) shows the average of the three temperatures measured in the radial direction—at the center of the tank, in the mid of the annulus between the helical heat exchanger and the tank wall, and on the tank wall—at eight evenly distributed vertical locations in the tank (Figure 4) during the test. T_mean_1 represents the average of the three temperature measurements at the bottom of the tank, and the numbers increase with vertical height until at location 8, which is at the top of the tank (T_mean_8). During the test, the temperature difference between the top and the bottom of the tank remains within 1 °C, while all the measured tank water temperature increased by 5.5 °C. The radial temperature distribution in the tank is shown in Figure 5(b). $MeanTemp_1$ represents the average of the eight evenly distributed temperature measurements at the center of the UTB. $MeanTemp_2$ and $MeanTemp_3$ are the average at the middle of the annulus and on the tank wall, respectively. The temperature differences among these vertical averages are within 0.25 °C throughout the test. These results indicate that the tank water is well-mixed in both the vertical and radial directions. Therefore, the tank was modeled as one single node.

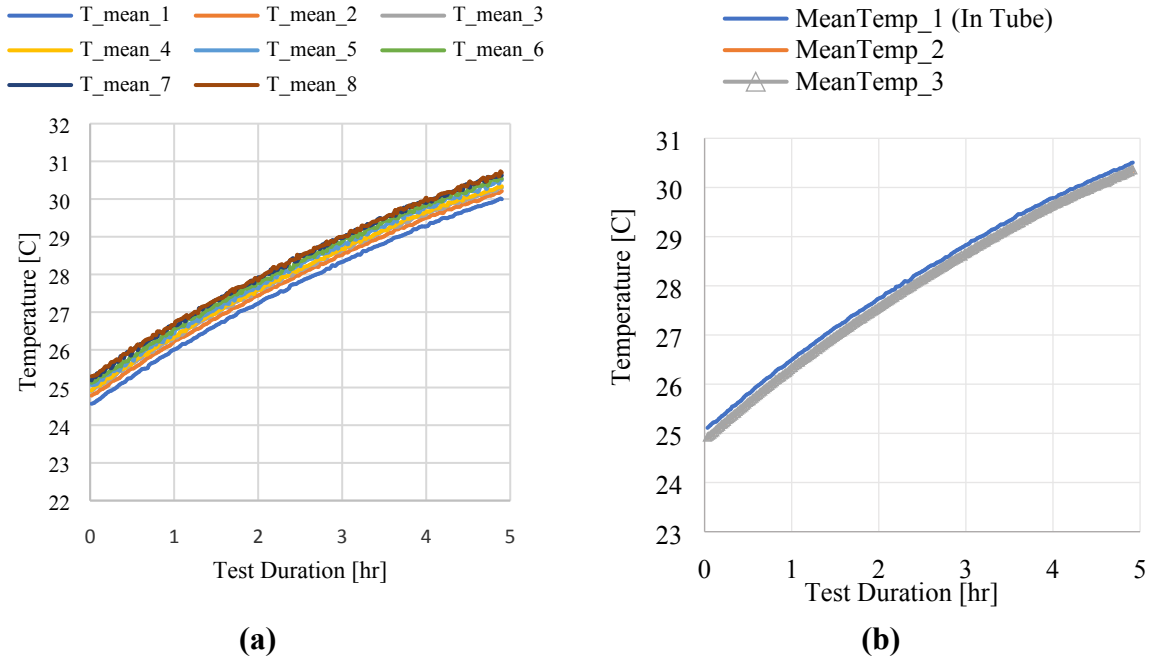


Figure 5. Measured temperature profiles in a small-scale UTB: (a) average temperature measured with three radially placed thermocouples at eight evenly distributed locations from the bottom to the top of the UTB; and (b) average temperatures measured with eight vertically located thermocouples at three radial locations.

The heat fluxes on the ground surface and the variation of soil temperature along the depth of the UTB were neglected and the annual mean soil temperature (T_m) was taken as an approximation of the initial condition of the simulated soil domain. The heat transfer in the soil is thus modeled as a 1D conduction problem. This simplification is because the annual variation (i.e., deviation from T_m) of the soil temperature decreases drastically with the depth of the soil, as shown in Figure 6. A sensitivity study is presented later in Section 4.2 to evaluate the impact of this simplification and its implication on the results of this study.

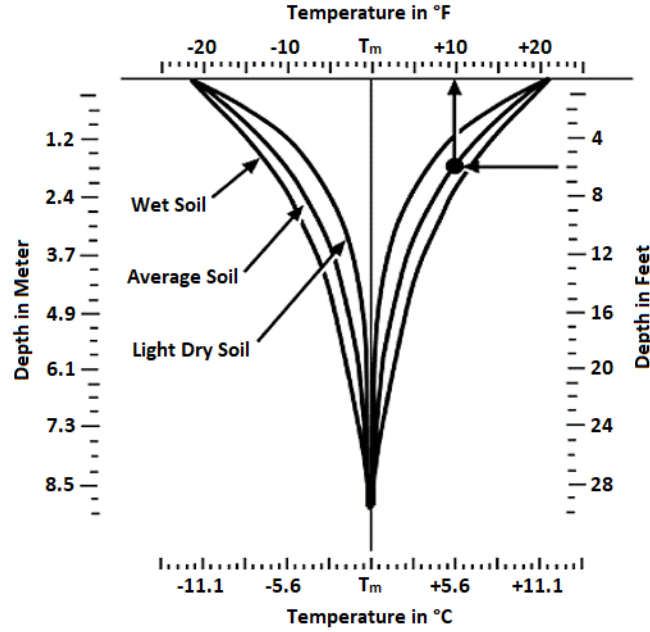


Figure 6. Temperature distribution in subsurface of soil (Adopted from Bose et al. 1985)

The heat transfer at the top and the bottom of the UTB is simplified by lumping the top and bottom surface area of the UTB into the side-wall of the UTB so that the entire surface area of the UTB is assumed at the same temperature. This simplification may result in some error in the heat transfer rate to the soil, and consequently the tank water temperature. However, as discussed later in Section 4, the error resulting from this simplification is not significant when compared with the simulation results of the detailed 3D model.

3.2 Model Structure

The 1D model consists of two modules—one for the PCM domain and one for the soil domain, as shown in Figure 7. For both the soil and PCM module, a finite volume method (FVM) is used to calculate the temperature change of each control volume (i.e., a hollow cylinder) at each time step. These modules calculate the heat transfer rate between the tank water and the soil (q_{soil}), and the heat transfer rate between the tank water and the PCM (q_{PCM}). While q_{soil} only includes sensible heat of the soil, q_{PCM} accounts for both the sensible and latent heat of the PCM.

Combining the heat input from the heat exchanger (q_{HEX}) with the heat exchanged with the PCM and the soil, the tank water temperature at a given time step T_i can be calculated with following heat balance equations (Equations 1 and 2). After the new tank temperature is calculated, the next iteration of the time loop begins until the simulation time is complete.

$$\Delta Q = q_{\text{HEX}} + q_{\text{PCM}} + q_{\text{soil}} \quad (1)$$

$$T_i = \frac{\Delta Q}{\rho V_{\text{UTB}} c_p} + T_{i-1} \quad (2)$$

where ρ and c are the density and specific heat of water; T_{i-1} is the tank water temperature at the last time step; V_{UTB} is the volume of the tank.

The benefit of this modular structure is that each module can be modeled with different meshes and can be separately changed to model different UTB designs without affecting the other parts of the model. This flexibility improves the computational efficiency and allows for optimizing design of the UTB, such as the selection of PCM (e.g., melting temperature and thermal properties), integration of the PCM (amount and layout of the PCM in the UTB), size of the UTB (number of tanks, diameter and depth of each tank). The optimization will be subject for further studies.

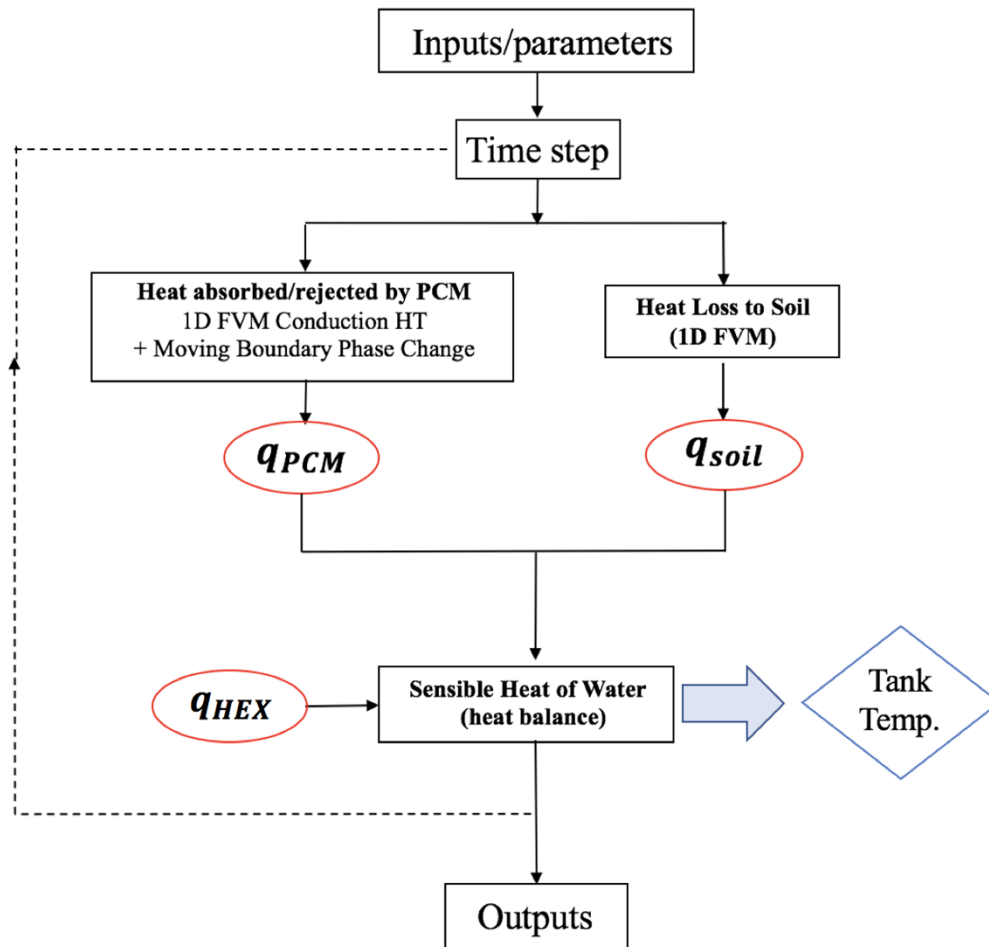


Figure 7. Flow diagram of the UTB model structure.

3.3 Simulation Domain

The simulation domain of the 1D model is depicted in Figure 8. Each node of the simulation domain represents the average temperature of a volume in the domain. The water tank is modelled as a cylinder that has a uniform temperature. It connects three subjects, including the helical heat exchanger, the surrounding soil, and the PCM. The heat exchanger provides constant or variable heat input to the tank. The surrounding soil is modelled as a series of hollow cylinders concentric to the UTB and the annular space of each hollow

cylinder has uniform thermophysical properties. The diameter of the simulated soil domain is 10 times the diameter of the UTB tank so that the heat transfer from the UTB is confined within the simulated soil domain. The boundary conditions for the soil domain consist of a variable temperature boundary at the tank wall, which is equal to the mean tank temperature (T_{tank}); and a constant temperature boundary at the perimeter of the soil domain, which is equal to the mean annual soil temperature ($T_{s,m}$). The soil domain (\vec{r}_s) is meshed with a logarithmic node spacing, such that the distance between each node increases as the node position becomes farther from the tank surface (r_1) until it reaches the domain boundary (r_2). This is given by the following expression:

$$\vec{r}_s = \frac{(r_2 - r_1)}{P} * 10^{\vec{u} - 1} + r_1 \quad (3)$$

where P is the exponential power of the logarithmic spacing, \vec{u} is a base vector consisting of n_s number of points linearly spaced between the bounds, which is determined with a MATLAB function—*linspace*, as expressed in Equation (4):

$$\vec{u} = \text{linspace}(0, \log_{10}(P + 1), n_s) \quad (4)$$

Since the heat transfer rate and the resulting soil temperature change diminishes along the radial direction of the soil domain, this expanding mesh of the soil domain allows for a reduction in the number of nodes without a loss of accuracy, thus reducing computation time.

The PCM domain is also modeled as a series of hollow cylinders concentric to the UTB. The mesh of the PCM domain has a linear node spacing given the small thickness of the PCM. A conduction boundary condition is applied to both sides of the PCM domain. The water is treated as a separate node with a spacing (same as that used in the PCM domain) from the PCM surface node. This node is substituted directly into the finite difference heat equation when solving for the surface node temperatures of the PCM.

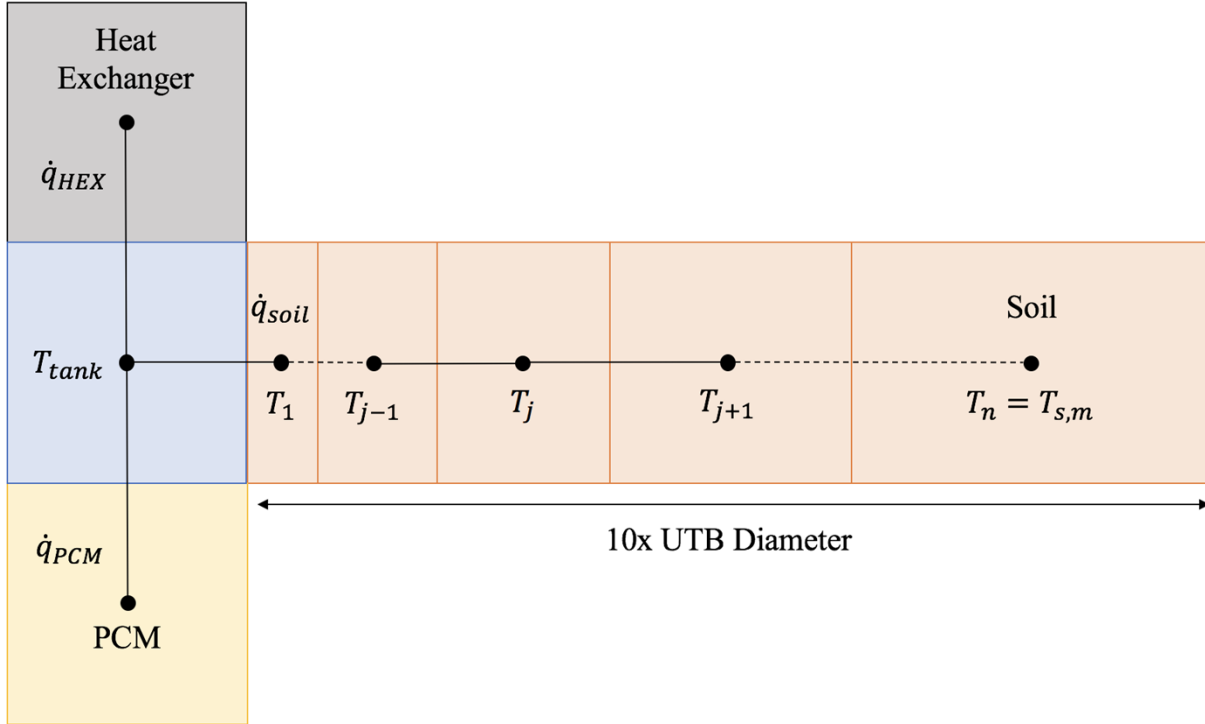


Figure 8. Simulation domain of a one-dimensional model of the underground thermal battery, where j is the spatial index of a soil node, n is the total number of soil nodes.

3.4 Governing Equations

The governing equations for the conduction heat transfer in the soil and the PCM, as well as the algorithm for modeling the phase change process of the PCM are presented in the following section.

3.4.1 Conduction Heat Transfer in Soil and PCM

The heat transfer in the soil and PCM is simplified as one-dimensional conduction heat transfer along the radial direction, which is expressed below in cylindrical coordinates (Equation 5):

$$\frac{\partial^2 T}{\partial r^2} + \frac{1}{r} \frac{\partial T}{\partial r} = \frac{1}{\alpha} \frac{\partial T}{\partial t} \quad (5)$$

where T is the temperature of a material (soil or PCM), t is the time, r is the radius from the center of the UTB, and α is the thermal diffusivity of the medium. Discretizing the above equation for explicit numerical calculation gives the following formula (Equation 6):

$$T_j^{i+1} = \alpha \Delta t \left[\frac{T_{j+1}^i - 2T_j^i + T_{j-1}^i}{\Delta r^2} + \frac{1}{r_j} \frac{T_{j+1}^i - T_{j-1}^i}{2\Delta r} \right] + T_j^i \quad (6)$$

where for a cell j and time step i : Δt is the temporal discretization, Δr is the spatial discretization, and r_j is the radius of the centerline of the cell.

Applying this formula to each finite control volume of the simulated material results in a set of equations. The solution of these equations is the temperature profile of the simulated material at a given time step. These equations are solved explicitly based on the calculated temperature profile in the previous time step and the heat fluxes (from the heat exchanger, soil, and PCM) at the current time step. The size of time step (Δt) is limited by the Cauchy stability criterion (Crank 1975) as expressed with Equation (7):

$$\Delta t < \Delta t_c = \frac{1\Delta r_{min}^2}{2\alpha} \quad (7)$$

where Δt_c is the critical time increment, and r_{min} is the minimum spatial increment. As it is desired to calculate the temperatures over a long simulation time, the maximum time step is chosen such that Δt is equal to $0.99\Delta t_c$.

3.4.2 Phase Change Process

The latent heat accumulation method proposed by Muhieddine et al. (2009) is adapted in this model to account for the latent heat which is released/absorbed during the phase change process. For simplicity, this model assumes that the melting temperature and the solidifying temperature of the simulated PCM are equal (i.e., a single temperature), neglecting the hysteresis effect of the PCM.

Because the PCM, which is enclosed in a panel made with thin plastic film, is suspended in the tank water, i.e., exchanging heat with the tank water at both sides of the PCM panel, two moving phase change interfaces develop within the PCM domain as the PCM temperature reaches its phase changing point and phase change occurs. Each interface is modeled with a control volume, within which phase change takes place at the constant phase change temperature. The PCM in this control volume is “mushy”, i.e., a mixture of solid and liquid PCM. For each time step during the phase change process, the energy transferred into this “mushy” volume is calculated based on a fictitious sensible heat, as expressed with Equation (8):

$$\Delta Q_j = \rho C(T_j^i - T_{pc}) \quad (8)$$

where T_j^i is a fictitious temperature of the “mushy” volume j at time step i ; T_{pc} is the phase change point; and C is the effective specific heat of the mixture of solid and liquid PCM, as expressed with Equation (9):

$$C = (1 - \theta_j^{i-1})c_l + \theta c_s \quad (9)$$

where θ_j^{i-1} is the fraction of solid material in volume j at last time step, c_l and c_s are the specific heats of the liquid and solid PCM, respectively. At end of the current time step i , the fraction of solid material is calculated with Equation (10) when PCM is melting, or Equation (11) when PCM is freezing:

$$\theta_j^i = 1 - \frac{\sum_1^i \Delta Q_j}{LH_j} \quad (10)$$

$$\theta_j^i = - \frac{\sum_1^i \Delta Q_j}{LH_j} \quad (11)$$

where LH_j is the maximum latent heat when all PCM in volume j completes phase change.

The fictitious sensible heat of time step i is then summed with each subsequent time step until the accumulated heat equals the maximum latent heat of the PCM in the volume. During this phase change process, the nodal temperature is reset to the phase change temperature after each time step before the temperature of the next control volume (T_{j+1}) is calculated. Once the accumulated heat equals the total latent heat of the PCM in the “mushy” volume j , this volume is no longer considered to be changing phase and the standard conduction equation is used to calculate the volume temperature during future time steps. Figure 9 shows a diagram of the PCM domain during a melting process. In this case, the water temperature is higher than the melting temperature of the PCM. The cells adjacent to the water melt and become liquid. Two “mushy cells” form in which the phase change occurs. In between the mushy cells is the solid region. This process is transient and can occur in reverse (i.e., freezing process) if the tank temperature drops below the phase change temperature of the PCM.

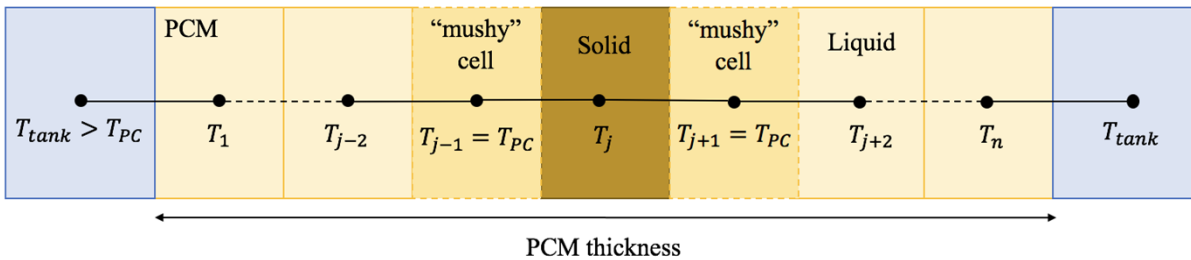


Figure 9. Diagram of PCM domain during phase change process.

4. MODEL VALIDATION

4.1 Validation against a Detailed 3D Model

A 3D and transient numerical model of the UTB was developed with a commercial software, ANSYS/FLUENT (version 17.2) by Zhang et al. (2019). The simulation domain of this 3D model is shown in Figure 10. It includes a cylindrical water tank buried in the ground, a helical coil heat exchanger, and a PCM sheet. The helical heat exchanger is at the center of the tank from the top to the bottom. A PCM sheet is immersed in the annulus between the tank wall and the heat exchanger. The PCM sheet is shorter than the tank so that there is enough space at both the top and bottom of the tank to allow water circulation, which is driven by the natural convection in the tank. The diameter of the simulated soil domain is 10 times the diameter of the UTB and adiabatic conditions are applied to the perimeter of the soil domain. As with the 1D model, it is assumed that the thermal properties of the soil are homogenous and constant, and there is not any contact resistance between the UTB wall and the surrounding soil. The ground surface heat flux and the soil temperature gradient along the UTB depth are modeled with the 3D model.

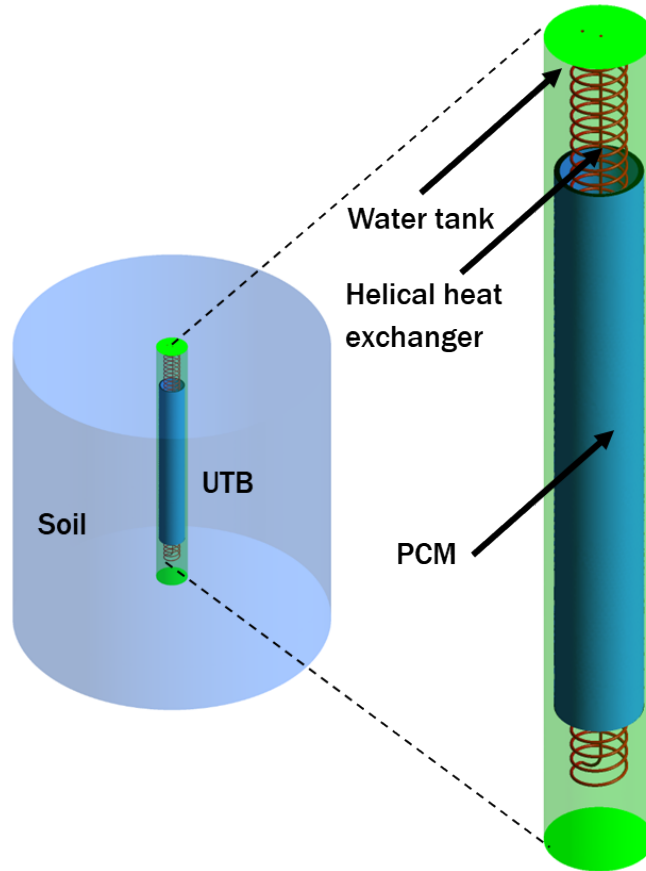


Figure 10. Simulation domain of a three-dimensional detailed numerical model for the UTB.

The 3D model accounts for both the heat transfer and the fluid dynamics within the UTB, as well as the conduction heat transfer in the surrounding soil. It can predict a detailed temperature profile in each component of the UTB at any given time. The results of the 3D model have been validated with experimental data of the small-scale UTB prototype. However, because of the complexity of the numerical calculations and the large size of the simulation domain, the 3D model is very time consuming and it was only used to predict the short-term (a few days) performance of the UTB (Zhang et al. 2019).

Simulation results of the 3D model is used to validate the 1D model. The dimensions and material thermophysical properties of the simulated full-size UTB are presented in Tables 2 and 3, respectively. The initial tank temperature is 295.9 K, just slightly below the 296 K melting temperature of the PCM. The initial soil temperature is 290 K. The heat input to the heat exchanger coil is 4,020 W for the first six hours (charging period) and there is not any heat input in the following 18 hours (recovery period).

Table 2. Geometry of the simulated underground thermal battery

Heat exchanger outer diameter (mm)	Heat exchanger inner diameter (mm)	Helical diameter (mm)	Tank length (m)	Tank diameter (m)	Soil length (m)	Soil diameter (m)	PCM thickness (mm)	PCM length (m)
28.85	22.45	381	6.71	0.76	7.93	7.62	80	4.47

Table 3. Materials thermophysical properties of the simulated underground thermal battery.

	Soil	Water	PCM	Copper
λ (W/(m·K))	1.72	0.6	1.09(solid)/0.54(liquid)	387.6
c_p (J/kg/K)	2121	4182	3140	381
ρ (kg/m ³)	1900	998	831.3	8978
T_{melt} (K)	--	--	296	--
L (kJ/kg)	--	--	200	--

Figure 11 shows that the tank water temperature predicted by the 1D model matches that predicted by the 3D model well if the same uniform temperature along the depth of soil is used in the 3D model. However, if the natural vertical temperature profile shown in Fig. 6 is accounted for in the 3D model (along with heat fluxes on the ground surface), its prediction of the tank water temperature is about 0.3°C higher than that predicted by the 1D model during the charging period (i.e., the first 6 hours with constant heat input) and the recovering period (without any heat input) except at the last 3 hours when the tank temperature predicted by the 1D model drops about 0.7 °C below what is predicted by the 3D model. The Root Mean Square Error (RMSE) between the tank temperatures predicted by the two models during the 24-hour time period is 0.1 °C if uniform temperature along the depth of soil is used in the 3D model. The RMSE increases to 0.3 °C if the natural temperature profile along the depth of the soil is modeled.

Figure 12 shows the liquid fraction of the simulated PCM domain, which is the mass ratio of the liquid PCM to the overall PCM mass (including both liquid and solid), predicted by the 3D and the 1D models through the 24-hour simulation period. The 1D model under-predicts the melting rate of the PCM relative to the prediction of the 3D Model, especially when the vertical soil temperature profile is accounted for in the 3D model. This disparity is consistent with the difference in tank temperature predicted by the two models. When accounting for the vertical temperature profile in the soil, the heat transfer rate to the soil becomes lower due to the smaller temperature difference between the tank water and the surrounding soil, which results in higher tank water temperature and faster melting rate of PCM during the charging period. The lower heat transfer rate also leads to slower temperature drop of the tank water and thus less PCM is solidified during the recovering period. It indicates that the melting/solidifying process of the PCM is sensitive to the vertical soil temperature profile. While the 1D model predicts a fully recovery of the PCM (all return to solid form) during 24 hours, the 3D model predicts that about half of the PCM is in liquid form after the same charging and recovering periods if the vertical soil temperature profile is taken into account. However, given the small difference in the predicted tank temperature between the two models, which determines the entering water temperature and efficiency of a GSHP, the 1D model is considered acceptable to predict the long-term performance of the UTB when it is used by a GSHP system as a heat sink and heat source.

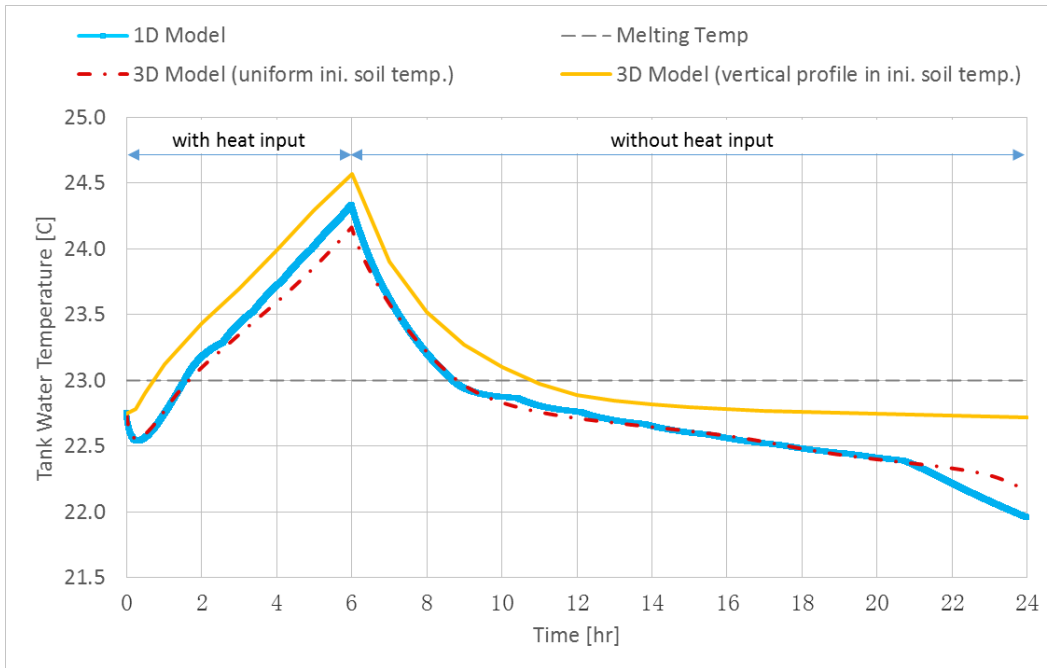


Figure 11. Temperature profiles for phase change simulation with 1D and CFD Model.

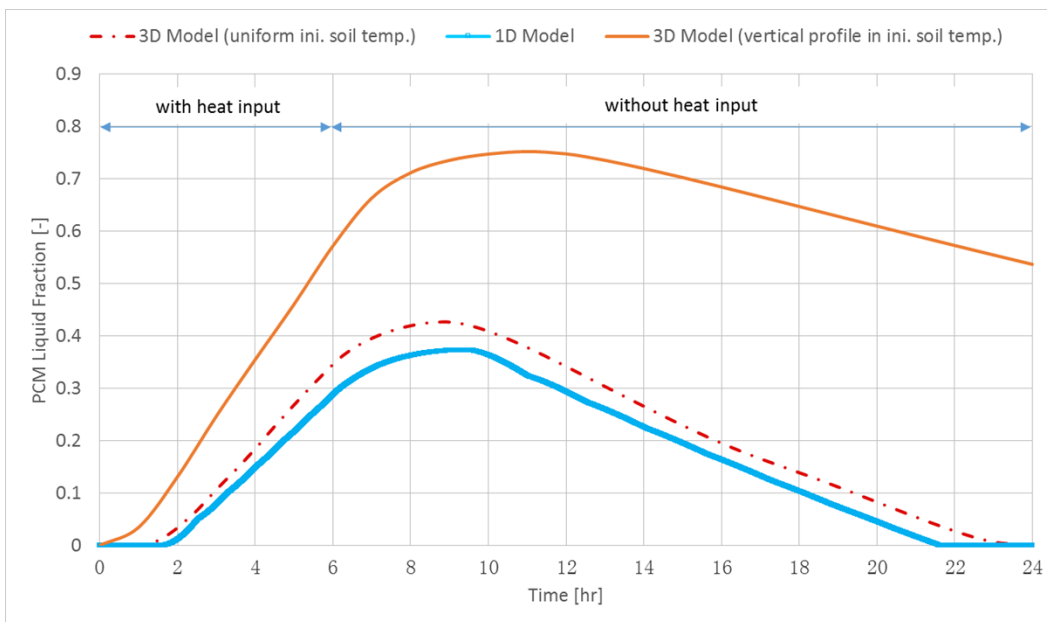


Figure 12. Liquid fraction of phase change material predicted by the 1D and 3D UTB models.

A comparison of the computation time between the 1D and 3D models was also conducted. The 3D model was able to simulate the performance of a full size UTB (Table 1) at a rate of approximately 1 minute of simulation per 1 minute of computation time. The total node count of the fine mesh used by the 3D model was approximately 3 million nodes. On the other hand, the 1D simulation required a much smaller mesh, with only a few hundred nodes. Therefore, it is much less computationally expensive than the 3D model.

The 1D model was able to simulate the full-size UTB at a rate of approximately 1 week of simulation time per 1 minute of computation time. This represents 10,000 times increase in computation efficiency.

4.2 Validation with Experimental Data

A lab test was performed to characterize the thermal response of the small-scale UTB (described in Section 2.1) when it was heated and the PCM was melting. The thermophysical properties of the PCM and other components of the UTB are listed in Table 3. During this test the UTB was exposed to the ambient air, which was maintained at about 22°C. The heat loss through the tank wall was measured with the four heat flux sensors installed on the outer surface of the tank. The UTB was heated through the helical heat exchanger with the electric heater. The heat input to the UTB was calculated with the measured the inlet and outlet temperatures, as well as the flow rate of the helical heat exchanger. The measured heat input and heat loss are shown in Figure 13. Figure 14 shows that the model-predicted tank water temperatures match the measured data fairly well. The root mean square error of the model prediction is 0.32 °C. To account for the time delay of the heat diffusion from the helical heat exchanger to the PCM, which was observed in the lab test, a diffusion fraction factor of 0.7 was applied in the 1D model. At each time step of the numerical calculation, the tank water and the heat input are divided into two parts: a fraction of the water is heated by the same fraction of the heat input and it exchanges heat with the PCM; while the rest of the water is heated by the rest of the input heat without exchanging any heat with the PCM. The average temperature of the two parts of water is calculated as the average tank water temperature at the time step.

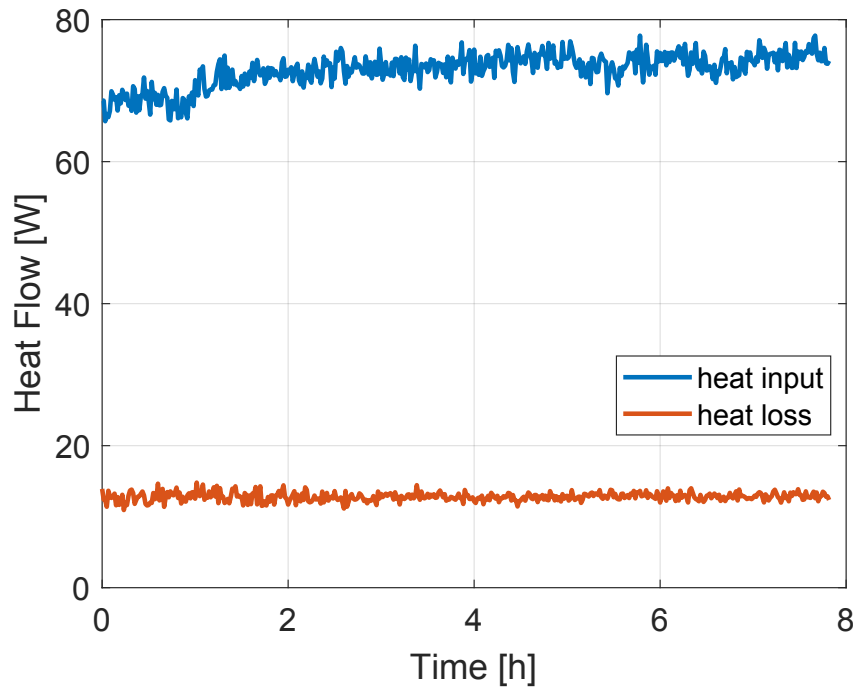


Figure 13. Measured heat input and heat loss during a lab test

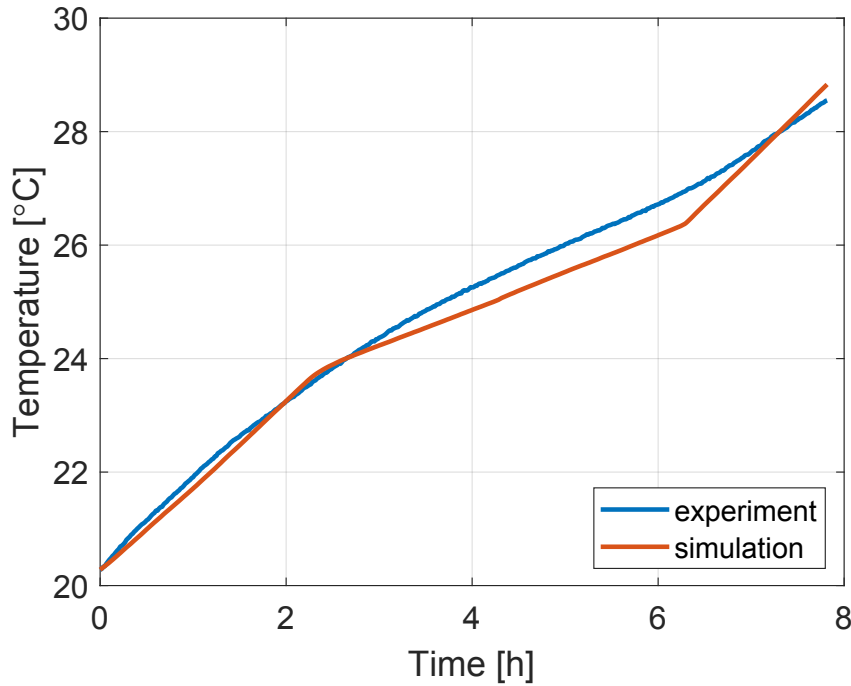


Figure 14. Measured and 1D model predicted tank water temperature

5. Preliminary Performance and Economic Analysis

A one-year simulation of the UTB was conducted to investigate its performance in response to thermal loads of a typical residential GSHP system. Figure 15 shows the leaving fluid temperature of a conventional VBGHE and that of a UTB, which has two parallelly connected water tanks. Dimensions of the simulated UTB and the VBGHE are listed in Table 4.

Table 4. Dimensions of conventional VBGHE and a full-scale UTB.

Dimension	VBGHE borehole	UTB (with 2 tanks)
Depth (m)	60.96	6.1 (each tank)
Diameter (m)	0.15	0.76 (each tank)
Volume (m ³)	1.08	2.77 (each tank)
Surface Area (m ²)	28.73	14.56 (each tank)
Surface area to volume ratio	26.6	5.26 (each tank)

The ground thermal conductivity is moderate at 2.63 W/m-K. The simulation is conducted using the hourly thermal load of a residential GSHP system with 1-ton capacity in Knoxville, TN. The thermal load is predicted using eQUEST version 3.6 (Hirsch and Gates 2017). The leaving fluid temperature of the VBGHE is also predicted with eQUEST. As shown in Figure 15, the leaving fluid temperature of the UTB changes little during daily operation. However, because of the relatively low temperature difference between the tank water and the surrounding soil, the UTB exchanges heat with the ground at a lower rate than the

conventional VBGHE. As a result, the thermal buildup in the tank, and eventually in the surrounding soil, causes the leaving fluid temperature of the UTB to increase over time. Despite the thermal buildup, the maximum leaving fluid temperature of the UTB is still comparable with that of the VBGHE in this case. Furthermore, the annual energy consumption of the GSHP system using the UTB is 2-5% less than that using the conventional VBGHE.

Simulation results indicate that the PCM only cycles between melting and freezing a few times in early summer and fall. After all the PCM is melted in the middle of July, the tank water temperature is above the melting temperature of the PCM (296 K or 23 °C) for several months, as shown in Figure 16, due to continuous heat rejection from the GSHP unit and the elevated temperature of the surrounding soil. This suggests that the PCM will not naturally cycle on its own and may therefore only be useful in applications in which there is active regulation of the UTB tank temperature so that the PCM can be cycled more frequently, e.g., on a daily basis.

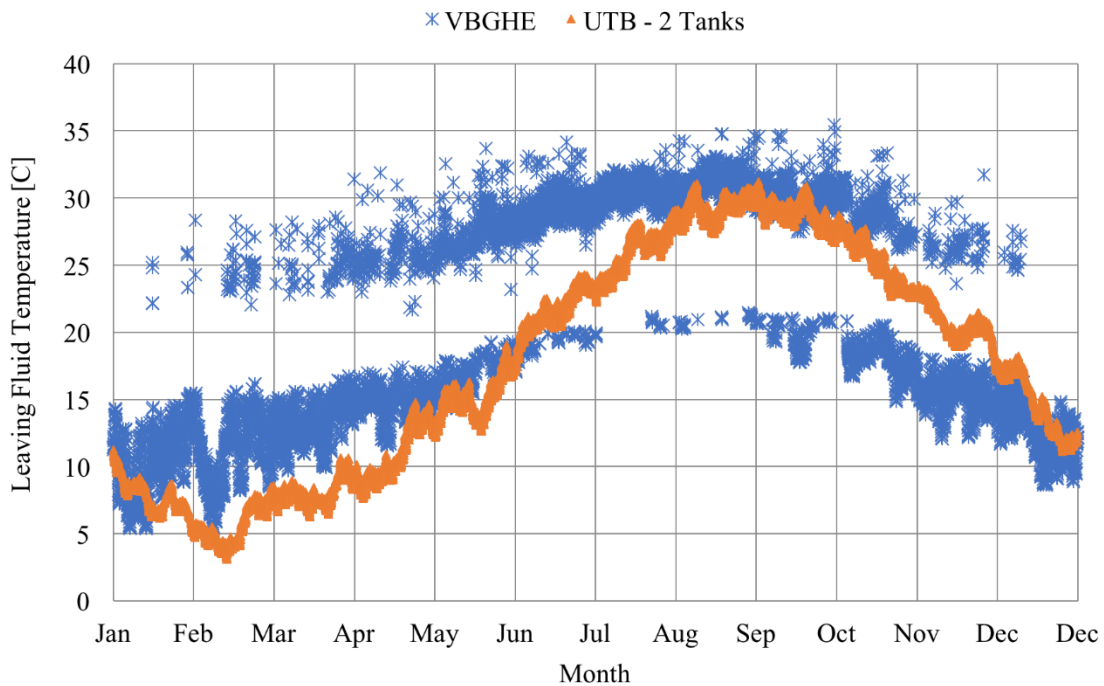


Figure 15. Comparison of simulation-predicted leaving fluid temperature between a UTB (with 2 tank) and a VBGHE during a one-year operation in Knoxville, TN and with moderate ground thermal conductivity.

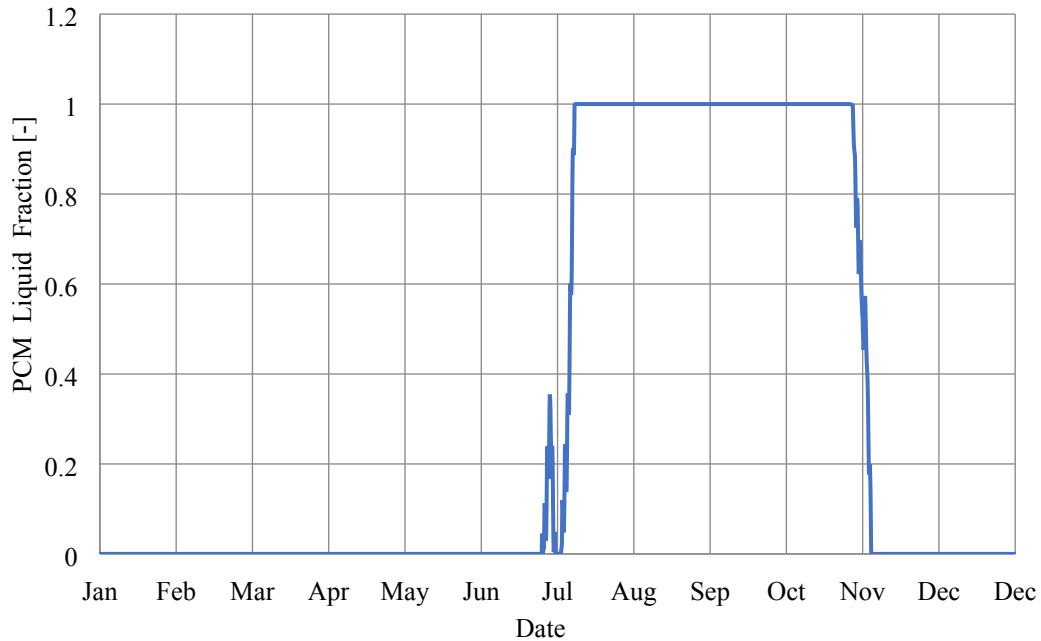


Figure 16. Liquid Fraction of PCM during a one-year operation of a residential ground source heat pump system in Knoxville, TN and with moderate ground thermal conductivity.

Figure 17 shows the annual heat pump electricity consumption resulting from using the VBGHE and the UTB under three effective ground thermal conductivities representing low, medium, and high values of typical ground formations. These results show that in the moderate Knoxville climate, using the UTB resulted in the similar heat pump power consumption as that resulting from using the VBGHE. The variation between annual heat pump power consumption with different ground thermal conductivities is not highly significant under moderate thermal loads, with an 8% increase between the low and high ground thermal conductivity. This result suggests that with proper sizing the ground thermal conductivity does not significantly affect the performance of the UTB.

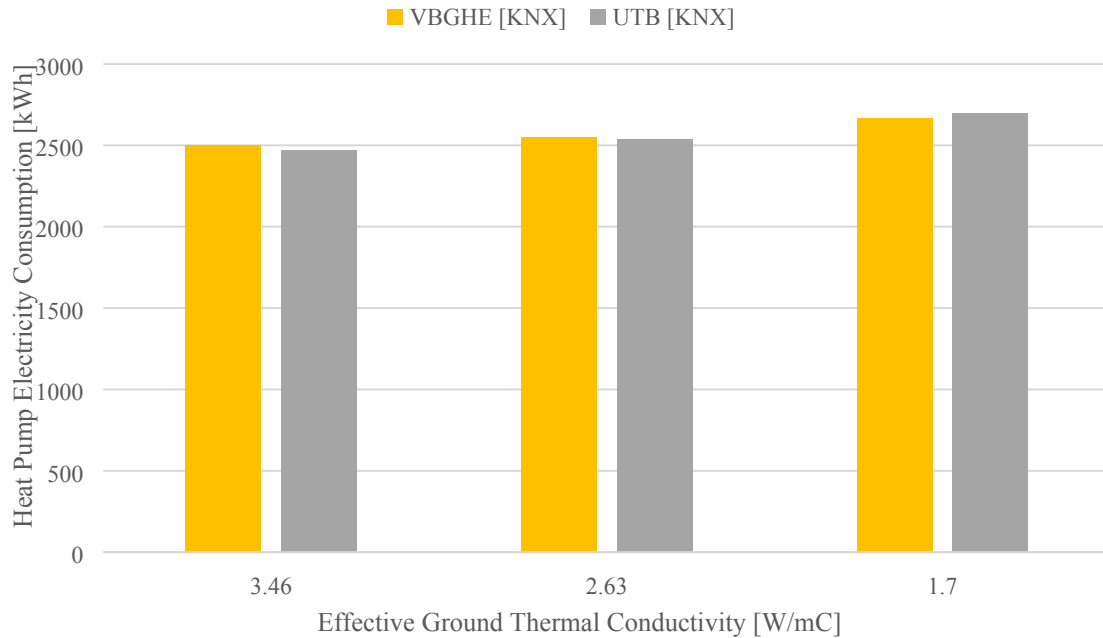


Figure 17. Comparison of the annual heat pump electricity consumption between a VBGHE and a UTB with two tanks under various effective ground thermal conductivities.

Cost data, presented in Table 5, was aggregated from various sources to develop a cost model for the UTB. This data includes retail prices for the various components as well as contractor estimates for drilling and installation. Auxiliary components (such as caps and connectors) were estimated at 5% of the cost of the tank and the helical heat exchanger. Corrugated Polyethylene pipes (36" or 24" diameter) are used to make the water tanks. One significant factor in the cost of a UTB is whether casing is needed to prevent borehole from collapse before the water tank is inserted in it. Both casing and non-casing scenarios are included in this analysis for purpose of comparison.

Table 5. Cost data for full-scale UTB.

Item	Unit Price	Supplier Type	Source
Corrugated Pipe 36"	\$836.99	Retail	(Agrisupply, 2019)
Corrugated Pipe 24"	\$454.99	Retail	(Agrisupply, 2019)
Helical Heat Exchanger (3/4" PVC)	\$139 /100 ft.	Retail	(McMaster Carr, 2019)
Auger Drilling (with casing)	\$61 /ft.	Contractor	(RSMeans 2010)
Auger Drilling (without casing)	\$21 /ft.	Contractor	(RSMeans 2010)
VBGHE installation	\$16 /ft.	Contractor	(Liu et al. 2019)

Figure 18 shows a cost comparison of a UTB with the conventional VBGHE as well as a conventional HVAC system for a two-ton cooling system. The results indicate UTB has significant cost reduction potential over the conventional VBGHE in the non-casing case. The installed cost of a UTB with two small tanks (24" diameter) is \$1,964 in this scenario, which is 39% lower than that of the VBGHE (\$3,200). The

installed cost of a UTB with single larger tank (36" diameter) is lower than that of a VBGHE even with casing; however it is a bit short of capacity to maintain the heat pump entering water temperature within the desirable range during annual operation. More comprehensive performance and cost analysis can be found in Warner (2019).

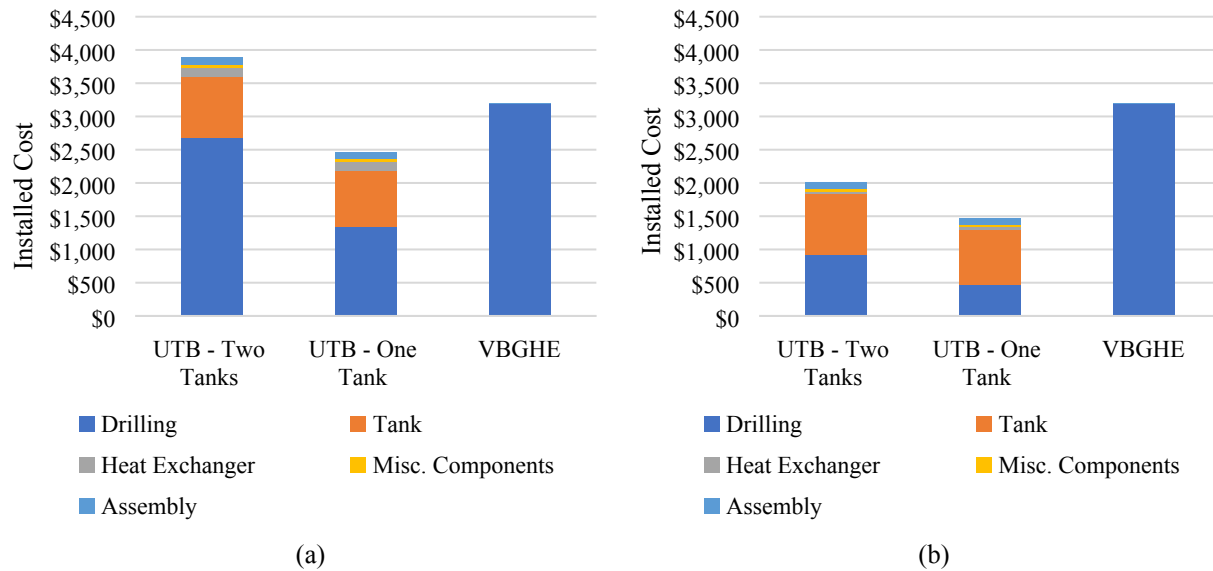


Figure 18. Cost of UTB (a) with casing and (b) without casing compared with a conventional vertical bore ground heat exchanger.

6. CONCLUSIONS

This paper presents a one-dimensional transient numerical heat transfer model of a novel ground heat exchanger, the Underground Thermal Battery (UTB). The 1D model was validated against both a more detailed 3D model and the experimental data of a small-scale UTB. The validation results indicate that:

- The 1D model can predict the temperature change of the UTB in response to a heat input with a similar accuracy as the detailed 3D model. However, the 1D model overpredicts the heat transfer rate to the surrounding soil and the associated melting/solidifying process of the PCM because it does not take into account the initial temperature gradient along the depth of the soil.
- The tank water temperature predicted by the 1D model matches the measured data fairly well after applying a diffusion fraction factor to account for the time delay of the heat diffusion from the helical heat exchanger to the PCM in the small-scale UTB.
- The computation efficiency of the 1D model is four orders of magnitudes higher than the 3D model due to its much smaller mesh count.

Given the small difference in the predicted tank temperature of the UTB between the 1D and the 3D models, which determines the entering water temperature and efficiency of a GSHP, and the high computation efficiency of the 1D model, it is considered acceptable to use the 1D model to predict the long-term performance of the UTB as a heat sink and a heat source of a GSHP system. The 1D model can be used to facilitate the design and optimization of the UTB for various applications.

A preliminary study utilizing the 1D model suggests that the performance of the UTB is comparable with an VBGHE that has the similar heat transfer surface area with the ground. However, the installed cost of

the UTB could be 39% lower than that of the VBGHE if casing is not needed for drilling the large diameter shallow boreholes.

Acknowledgement

The authors thank the Emerging Technologies Program of the Buildings Technology Office at the U.S. Department of Energy for supporting this research project

REFERENCES

Agrisupply, (2019). Retrieved from www.agrisupply.com.

Al-Khoury, R., Bonnier, P., Brinkgreve, R., 2005. Efficient finite element formulation for geothermal heating systems. Part I: steady state. *International Journal of Numerical Methods in Engineering* 63 (7), 988-1013.

Bertermann, David, Bernardi, A., Pockelé, L., Galgaro, A., Cultrera, M. D., and Müller, J., 2018. European Project ‘Cheap-GSHPs’: Installation and Monitoring of Newly Designed Helicoidal Ground Source Heat Exchanger on the German Test Site. SpringerLink, Springer, Dordrecht, 27 Dec. 2018, link.springer.com/article/10.1007/s12665-018-7343-4.

Bose, J., J. Parker, and F. McQuiston. 1985. *Design/Data Manual for Closed-loop Ground-coupled Heat Pump Systems*. American Society of Heating, Refrigerating and Air-Conditioning Engineers, Inc.

CDH Energy Corp. (Frontier Energy). 2017. Final Report for Analysis of Water Furnace Geothermal Heat Pump Sites in New York State with Symphony Monitoring System. Submitted to New York State Energy Research and Development Authority.

Crank, J. *The Mathematics of Diffusion*. 2nd Edition, Oxford, 1975, p. 143.

Cordts, D., 2011. The GeoColumn™ Geothermal Heat Pump Company. Geothermal Energy Workshop. April 13, 2011.

D&R International. 2012. *Buildings Energy Data Book* (U.S. Department of Energy).

Eskilson, P. and Claesson, J., 1988. Simulation model for thermally interacting heat extraction boreholes. *Numerical Heat Transfer* 13: 149-165.

F. W. Webb (2019). Retrieved from www.fwebb.com

Gonthier, S., 2012. GEOPERFORMX Thermally Enhanced Pipe for Geothermal Applications., 2012 Annual Conference of International Ground Source Heat Pump Association. October 4th, 2012.

Hirsch, J. and S. Gates. 2017. eQUEST Version 3.65 (<http://www.doe2.com/equest/>).

Im, P., Hughes, P., and Liu, X., 2012. Demonstration and performance monitoring of foundation heat exchangers (FHX) in ultra-high energy efficient research homes. Proceedings of the 2012 ACEEE Summer Study on Energy Efficiency in Building, August, Pacific Grove, CA

Ingersoll, L. R., Zobel, O.J. and Ingersoll, A.C. 1954. *Heat conduction with engineering, geological and other applications*. McGraw-Hill, New York.

Jensen, R., 2014. TWISTER High Efficiency Geothermal Heat Exchanger. 2014 Annual Conference of International Ground Source Heat Pump Association. Baltimore, Maryland.

Lamarche, L. and Beauchamp, B. 2007. A new contribution to the finite line-source model for geothermal boreholes. *International Journal of Heat and Mass transfer* (5097-8): 1408-1419.

Liu, Z., W. Xu, X. Zhai, C. Qian, and X. Chen., 2017. “Feasibility and performance study of the hybrid ground-source heat pump system for one office building in Chinese heating dominated areas,” *Renew. Energy*, vol. 101, pp. 1131-1140, 2017.

Liu, X., Y. Polsky, D. Qian and J. McDonald. 2018. Analysis of Cost Reduction Potential of Vertical Bore Ground Heat Exchanger. ORNL/TM-2018/756. Oak Ridge, TN: Oak Ridge National Laboratory

Liu, X., P. Hughes, K. McCabe, J. Spittler, and L. Southard. 2019. GeoVision Analysis Supporting Task Force Report: Thermal Applications—Geothermal Heat Pumps. ORNL/TM-2019/502. Oak Ridge, Tennessee: Oak Ridge National Laboratory.

McMaster Carr (2019). Retrieved from www.mcmaster.com.

Muhieddine, M., Canot, É, & March, R., 2009. Various Approaches for Solving Problems in Heat Conduction with Phase Change. *International Journal on Finite Volumes*,6(1).

NYSERDA (New York State Energy Research and Development Authority). 2017. Renewable Heating and Cooling Policy Framework.

(Available at <https://www.nyserdera.ny.gov/-/media/Files/Publications/PPSER/NYSERDA/RHC-Framework.pdf>)

Palm, B., and M. Ignatowicz., 2016. “Adsorption Corrosion Inhibitors, Green Corrosion Inhibitors and Alternative Secondary Fluids for Indirect Systems.” Retrieved 7/15/2016, from <http://effsysexpand.se/p03-adsorberande-korrosionsinhibitorer/>.

RSMeans. 2010. RSMeans Mechanical Cost Data 2010. Kingston, MA.

Tiedje, E. and P. Guo. 2014. “Thermal Conductivity of Bentonite Grout Containing Graphite or Chopped Carbon Fibers.” *Journal of Materials in Civil Engineering* 26(7), [https://doi.org/10.1061/\(ASCE\)MT.1943-5533.0000977](https://doi.org/10.1061/(ASCE)MT.1943-5533.0000977).

Water Research Foundation. 2016. Residential End Uses of Water, Version 2. Retrieved from Water Research Foundation: <http://www.waterrf.org/PublicReportLibrary/4309A.pdf>

Warner, J. 2019. Feasibility Study of a Novel Ground Heat Exchanger using Phase-Change Materials. (Master’s thesis). The University of Tennessee, Knoxville, Tennessee. Available at the Tennessee Research and Creative Exchange (TRACE).

Yavuzturk, C. 1999. Modelling of vertical ground loop heat exchangers for ground source heat pump systems. Doctoral thesis, Oklahoma State University, USA.

Zacchei, M., 2016. GEOthermal Technology for Economic Cooling and Heating. D7.1 Market Assessment. GEOTECH.

Zhang, M., X. Liu, K. Biswas and J. Warner. 2019. A 3D Numerical Investigation of a Novel Shallow Bore Ground Heat Exchanger Integrated with Phase Change Material. *Applied Thermal Engineering* 162 (2019) 114297. <https://doi.org/10.1016/j.applthermaleng.2019.114297>